Stable Nonspherical Fluorine-Containing Colloidal Dispersions: Synthesis and Film Formation

W. Reid Dreher, William L. Jarrett, and Marek W. Urban*

Department of Polymer Science, School of Polymers and High Performance Materials, Shelby F. Thames Polymer Science Research Center, The University of Southern Mississippi, Hattiesburg, Mississippi 39401

Received October 8, 2004; Revised Manuscript Received December 16, 2004

ABSTRACT: A simple synthetic method for preparing stable colloidal dispersions that form polymeric films containing fluorinated acrylates is presented. The simultaneous presence of the dual tail anionic fluorosurfactant phosphoric acid bis(tridecafluorooctyl) ester ammonium salt (FSP) and sodium dodecyl sulfate (SDS) surfactants facilitates a suitable environment for the aqueous polymerization of methyl methacrylate/*n*-butyl acrylate/heptadecafluorodecyl methacrylate (MMA/nBA/FMA) colloidal particles. Polyermerization is achieved by a low-sheer monomer-starved emulsion polymerization process in which the FSP/SDS surfactant mixture significantly reduces the surface tension of the aqueous phase, thus facilitating mobility and subsequent polymerization of FMA along with MMA and nBA momomers. Using this approach, it is possible to obtain stable nonspherical MMA/nBA/FMA colloidal dispersions containing up to a 8.5% (w/w) copolymer content of FMA. These studies illustrate that the incorporation of FMA into MMA/nBA particle morphologies facilitates surface phase separation during coalescence, resulting in F-containing film−air (F−A) interfaces. Thus, surface properties with a significant decrease in the kinetic coefficient of friction as well as high contact angles can be produced.

Introduction

The incorporation of F-containing monomers into polymeric systems has been of considerable interest for a number of years due to the fact that their presence may introduce a number of unique physical and chemical properties.[1−11] As a consequence, F-containing polymers exhibit numerous applications ranging from hollow bodies and moldings to fibers, composite materials, films, and foams. While such properties as thermal stability and chemical resistance are expected to be enhanced, decreases in surface tension and friction are consequences resulting from the presence of F-containing species.[12−14] However, exceptionally reduced surface tension and solubility in aqueous environments make synthetic efforts quite challenging, and potential adverse effects on the formulation of continuous polymeric films are also anticipated.

Although there are obvious advantages and benefits in generating F-containing polymers via emulsion polymerization, their incorporation into colloidal particles is not straightforward. The primary reason is the immiscibility between hydrophobic C−F entities and the continuous aqueous phase resulting from large surface tension differences. Due to the fact that traditional emulsion polymerization relies on the diffusion of monomers from monomer droplets through the aqueous phase to micelles for polymerization to occur, this process often limits the concentration levels of F-contaning species.[15] Several synthetic attempts[12,16−36] have been made to produce F-containing colloidal dispersions in which organic solvents, high shear rates, homogenizers, fluorinated surfactants, and sonication techniques were utilized to facilitate monomer diffusion through an aqueous phase. Although these approaches have been somewhat successful, their preparation can be quite elaborate even with relatively low F content, thus inhibiting desirable film properties. Another approach to increase the F content of colloidal dispersions was to incorporate F-containing acrylates into colloidal particles, which have shown desirable properties. The presence of the pendant $-CF_3$ end groups on the perfluoroalkyl side chains appears to generate surface tensions even lower than those of the corresponding poly(tetrafluoroethylene) ($-CF_2-$) polymers[37,38] and their derivatives.[36]

Despite numerous difficulties and challenges in incorporating F-containing species into colloidal dispersions, there are also opportunities. The current studies offer a simple synthetic approach which utilizes monomer-starved conditions implemented during a classical emulsion polymerization process to produce controlled colloidal particles containing methyl methacrylate (MMA), *n*-butyl acrylate (nBA), and heptadecafluorodecyl methacrylate (FMA) in the presence of sodium dodecyl sulfate (SDS) and phosphoric acid bis(tridecafluorooctyl) ester ammonium salt (FSP). Both surfactants facilitate the necessary conditions to allow F-containing monomer diffusion through the aqueous phase to micelles, subsequently allowing copolymerization of FMA, MMA, and nBA species. The second part of this publication focuses on film formation processes from such F-containing colloidal particles and the effect of particle morphologies on stratification during coalescence.

Experimental Section

MMA, nBA, FMA, potassium persulfate (KPS), and SDS were all purchased from Aldrich Chemical Co. FSP was received from DuPont. The structures of SDS and FSP surfactants are shown below.

All colloidal dispersions were synthesized under monomer-starved conditions using a semicontinuous polymerization process in which all monomers and surfactants were dissolved in water and stirred under high agitation to produce a semistable pre-emulsion.[35] A 10% (w/w) concentration of the

* To whom correspondence should be addressed.

10.1021/ma0479161 CCC: $30.25
Published on Web 02/08/2005

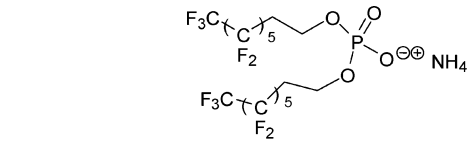

FSP

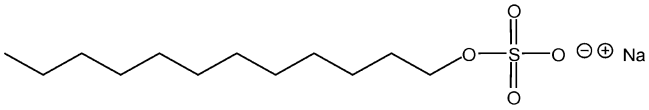

SDS

pre-emulsion and an 18% (w/w) concentration of the initiator solution were injected into the reaction kettle, which contained 100 g of water. This process facilitates the seeding of the emulsion polymerization. The mixture was then stirred for 30 min to allow for initiation reactions to occur. The remaining pre-emulsion was fed continuously over 3.5 h, and the initiator solution was fed over 4 h. Upon the completion of the initiator feed, polymerization was allowed to continue for an additional 5 h. Polymerization reaction was carried out in a 1 L reaction kettle equipped with a reflux condenser at 79 °C in a N_2 atmosphere under continuous agitation (300 rpm) using a Caframo BDC3030 digital stirrer. Particle size measurements were obtained using a Microtrac UPA 250, and Table 1 lists the resulting particle sizes, percent solids (w/w), and concentration levels of individual components. As listed, specimen A represents MMA/nBA colloidal dispersions prepared in the presence of SDS, and specimen B is MMA/nBA prepared using SDS/FSP surfactants. The same SDS/FSP mixture was used to prepare specimens C, D, and E, which contain 3.3%, 5%, and 8.5% w/w FMA copolymer, respectively. Such prepared colloidal dispersions were cast on a poly(vinyl chloride) (PVC) substrate and allowed to coalescence at 50% relative humidity (RH) for 3 days at 23 °C to form approximately 20 μm thick films. Film thickness was determined by using a Pro Max caliper.

Polarized attenuated total reflectance Fourier transform infrared (ATR-FTIR) spectra were collected using a Bio-Rad FTS-6000 FTIR single-beam spectrometer set at a 4 cm^{-1} resolution which was equipped with a ZnSe polarizer. A 45° face angle Ge crystal with 50 × 20 × 3 mm dimensions was used. The use of a ZnSe polarizer facilitates orientation studies by utilizing TE (transverse electric) and TM (transverse magnetic) modes of polarized IR light. Each spectrum represents 100 co-added scans ratioed against the same number of reference scans collected using an empty ATR cell. All spectra were corrected for spectral distortions and optical effects using Q-ATR software.[39,40]

Transmission electron micrographs were acquired on a Zeiss EM 109T microscope using an accelerating voltage of 80 kV. Samples of colloidal dispersion used for transmission electron microscopy (TEM) analysis were prepared by making a 1:10000 dilution in deionized water followed by casting onto Formvar-coated copper grids (Ted Pella, Inc.). Particle size and particle size distribution measurements were performed using a Microtrac UPA 250.

Atomic force microscopy phase images (Nanoscope IIIa Dimension 3000 scanning probe microscope, Digital Instruments) were obtained using a Si cantilever at a resonance frequency around 300 kHz. Solid-state ^{13}C NMR spectroscopy was performed on a Varian ^{UNITY}INOVA 400 spectrometer using a standard Chemagnetics 7.5 mm PENCIL-style probe. Samples were loaded into zirconia rotor sleeves, sealed with Teflon caps, and spun at a rate of 4.5 kHz. The standard cross-polarization/magic angle spining (CP/MAS) technique was used with high-power proton decoupling implemented during data acquisition. The acquisition parameters were as follows: The ^1H 90° pulse width was 4.0 μs, the cross-polarization contact time was 1 ms, the dead time delay was 6.4 μs, and the acquisition time was 45 ms.[41] A recycle delay of 3 s between scans was utilized. Experiments requiring simultaneous ^1H and ^{19}F decoupling were performed using a 3.2 mm HFXY probe. The ^1H and ^{19}F 90° pulse widths were 4.0 μs, the acquisition time was 26 ms, and the $^{19}F-^{13}C$ cross-polarization contact time was 1 ms. A recycle delay of 2 s and a samples spinning rate of 5 kHz were used.

Surface tension measurements of polymeric films and solutions were conducted by using an FTA200 dynamic contact angle analyzer and a KRUSS K12 process tensiometer, respectively. A Qualitest 1055 friction tester was utilized to determine the kinetic coefficient of friction,[42] and each film was subjected to MEK double rubs[43] to determine solvent resiliency.

Results and Discussion

As indicated in the Introduction, the synthesis of F-containing colloidal dispersions may be troublesome because water−monomer miscibility in the presence of a F-containing monomer is low due to the hydrophobic nature of the fluorinated species. To overcome these difficulties, we developed a simple synthetic procedure that allows the incorporation of F-containing monomers into MMA/nBA copolymer particles by utilizing an SDS/FSP surfactant mixture. This approach facilitates the reduction of the surface tension of the aqueous phase, thus increasing the ability of the F-containing monomer to diffuse into micelles. For example, the addition of 0.98% SDS (w/w aqueous solution) decreases the surface tension of the aqueous phase from 73 to 38 mN/m, and polymerization reactions conducted under these conditions in the presence of FMA generate colloidal dispersions containing a large degree of coagulum. On the other hand, the addition of SDS along with FSP (0.98% and 0.62% w/w aqueous solution, respectively) further reduces the surface tension of the aqueous phase to 19 mN/m. These conditions, as described in the Experimental Section, provide a suitable environment for the synthesis of MMA/nBA/FMA copolymer particles containing up to 8.5% (w/w) FMA monomer.

In an effort to determine that indeed FMA was incorporated into MMA/nBA/FMA colloidal particles, we

Table 1. Composition of F-Containing Colloidal Dispersions Based on Final Latex Weight[a]

	colloidal disperson compositions				
	specimen A	specimen B	specimen C	specimen D	specimen E
[FMA] (% w/w)	0	0	1.22	1.94	3.27
[MMA] (% w/w)	18.9	18.9	18.3	18.8	18.1
[nBA] (% w/w)	18.3	18.3	17.7	18.1	17.4
[SDS] (%w/w)	0.61	0.61	0.61	0.60	0.60
[FSP] (% w/w)	0	0.97	0.97	0.95	0.95
[KPS] (% w/w)	0.23	0.23	0.23	0.22	0.22
[DDI] (% w/w)	61.96	60.96	60.97	59.39	59.46
particle size (nm)	91	94	97	102	104
% solids	45	42	41	43	42

[a] Also shown are particle size measurements, and % solids (w/w) of colloidal dispersions.

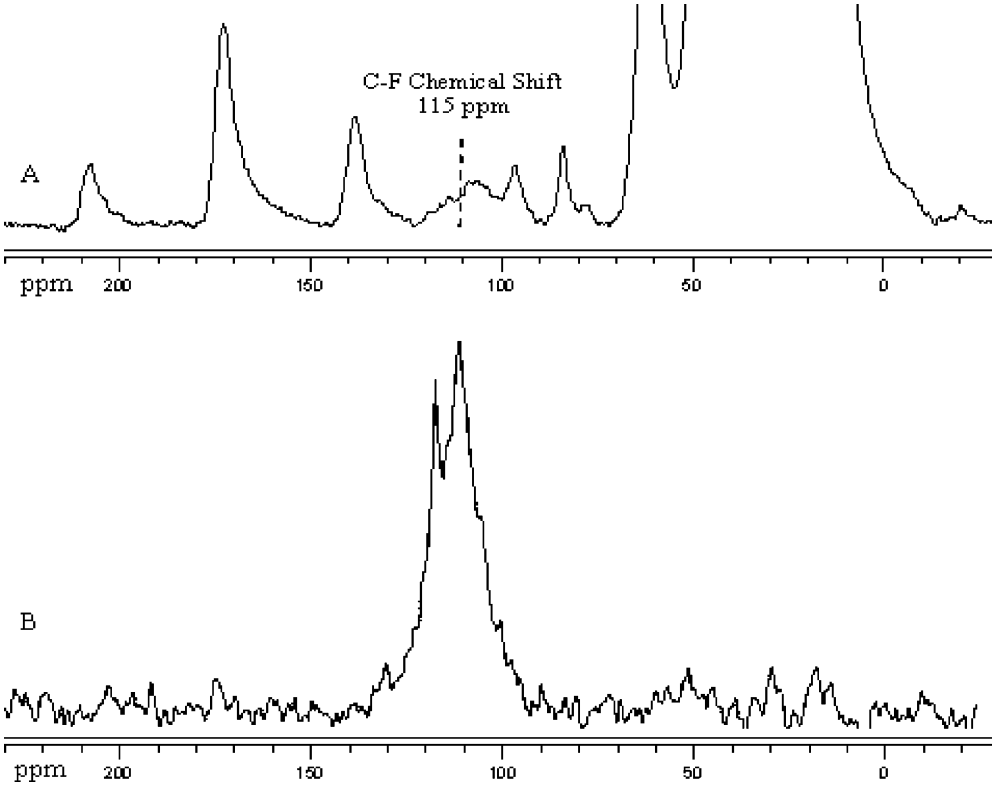

Figure 1. Solid-state NMR spectra of MMA/nBA/FMA copolymer films: (A) ^{13}C NMR spectrum; (B) ^{19}F and ^{13}C cross-polarized experiments with ^{1}H and ^{19}F decoupling.

utilized NMR spectroscopy. Specifically, solid-state NMR was employed as a means to detect polymer microstructure, and Figure 1, trace A, represents a solid-state ^{13}C spectrum of MMA/nBA/FMA. Although the presence of the perfluoroalkyl side chain of FMA is detected at 115 ppm,[44] this technique alone only allows us to determine that FMA is a bulk entity in the film. To enhance selectivity of NMR analysis along with increasing polymer microstructure information, we utilized cross-polarization of ^{19}F to ^{13}C along with the decoupling of ^{1}H and ^{19}F nuclei.[45] This technique facilitates through-space experiments, and furthermore, by the decoupling of ^{1}H and ^{19}F nuclei, the resulting spectrum will be indicative of functional groups in close proximity of the perfluoroalkyl side chains. As shown in Figure 1B, the C−F band at 115 ppm is the only functional group detected, and due to the fact that this is a through-space- and not bond-to-bond-dependent experiment, these data show that the polymeric microstructure consists of MMA/nBA and FMA domains. The smaller peaks at 221.5, 132, 97, and ~87 ppm are spinning sidebands due to the MAS technique.

Thus, two possibilities exist: (1) MMA/nBA and FMA formed two separate particles, or (2) MMA/nBA/FMA particle morphologies are such that there is a phase separation between MMA/nBA and FMA within the same particle. To determine if indeed FMA exists as a separate colloidal particle, we analyzed the particle size data listed in Table 1. As seen, the particle size of MMA/nBA/FMA (8.5% w/w FMA) is 104 nm, and it exhibits a monomodal distribution of particles, thus indicating one-size particles. To further verify that FMA does not polymerize as a separate entity, we synthesized FMA homopolymer particles under the same conditions, which was accomplished by utilizing the same formulation and synthetic procedures as for MMA/nBA/FMA (8.5% w/w), but without MMA or nBA. The results of this experiment are shown in Figure 2, where trace A represents the particle size distribution for FMA homopolymer, and trace B is MMA/nBA/FMA (8.5% FMA w/w). As seen, the synthesis of FMA homopolymer produces a monomodal distribution of particles with an average diameter of 26 nm, and MMA/nBA/FMA colloidal particles (trace B) exhibit an average size of 104 nm with a monomodal distribution. Therefore, if two particle sizes consisting of MMA/nBA and FMA were obtained during polymerization reactions, bimodal particle size distribution would be observed. Thus, the particle size and solid-state NMR data, as well as the fact that the obtained dispersions exhibit good shelf stability, monomodal particles consist of MMA, nBA, and FMA, but compared to randomly polymerized MMA and nBA, the FMA phase is polymerized as a block.

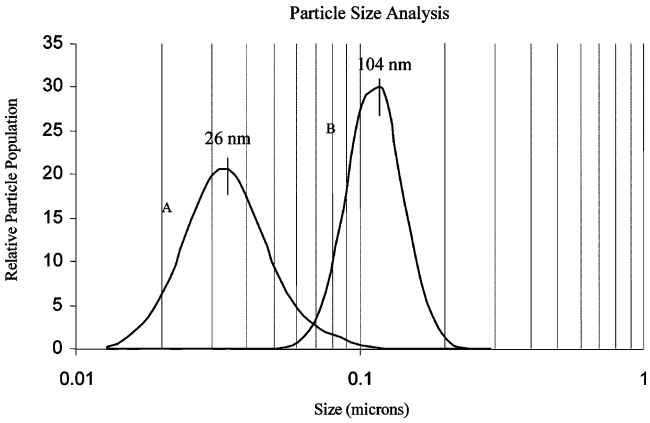

Figure 2. Particle size distribution: (A) FMA homopolymer; (B) MMA/nBA/FMA (8.5% w/w FMA).

As a means to establish how MMA/nBA/FMA is able to polymerize to form monomodal particles, we utilized TEM. The results of these experiments are displayed

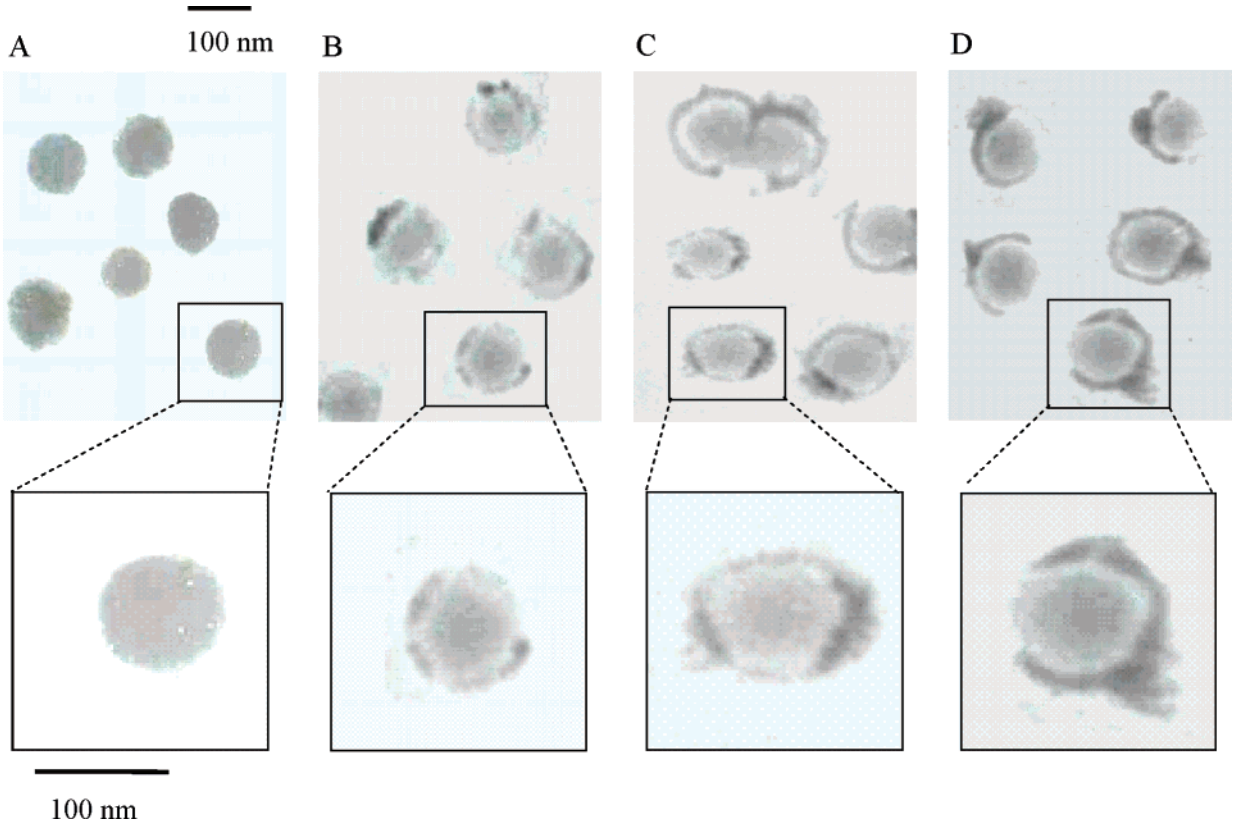

Figure 3. Transmission electron micrographs: (A) MMA/nBA; (B) MMA/nBA/FMA (3.3% w/w FMA); (C) MMA/nBA/FMA (5% w/w FMA); (D) MMA/nBA/FMA (8.5% w/w FMA).

in Figure 3 for MMA/nBA (A), MMA/nBA/FMA (3.3% w/w) (B), MMA/nBA/FMA (5% w/w) (C), and MMA/nBA/FMA (8.5% w/w) (D). As shown in Figure 3A, MMA/nBA colloidal particles exist as monomodal entities with no considerable electron density changes, indicating expected random copolymerization. On the other hand, the incorporation of 3.3%, 5%, and 8.5% (w/w) FMA (Figure 3B–D) results in colloidal particles of a similar size, but the particles exhibit two significantly different electron densities and shapes. As shown in Figure 3B, the presence of 3.3% FMA in MMA/nBA colloidal particles results in high electron density regions near the exterior of the particles, and by increasing the FMA copolymer content (Figure 3B,C), the size of these domains increases and they change shape from spherical (Figure 3A) to lemon-shaped with the ends containing FMA. Thus, these experiments confirm earlier predictions and indicate that the pFMA phase is polymerized on the exterior of pMMA/nBA particles, resulting in a nonspherical particle shape. This non-core–shell morphology might play a significant role during coalescence because if core–shell spherical morphologies were obtained such that the shell would constitute FMA, such particles would not easily, if at all, coalesce due to the very high T_g of the pFMA phase (172 °C).

In view of the above experimental data, the question is how reactivity ratios of monomers and employed synthetic procedures allow us to overcome "nonfavorable" synthetic conditions. As indicated earlier, reduction of surface tension is one aspect, but the reactivity ratios of MMA and nBA are 39 and 23 with respect to FMA,[46] whereas for MMA with nBA, $r_1 = 1.7$ (MMA) and $r_2 = 0.34$ (nBA).[47] (Reactivity ratios of FMA with MMA and nBA were calculated by utilizing Q and e values for MMA, nBA, and tetrafluoroethylene (TFE). No FMA values are available in the literature, and the Q and e values for TFE were used.) During the initial stages of polymerization, MMA and nBA form random copolymer particles, and by starving the system of monomer radicals, FMA is able to add onto the existing particles at a later stage during the polymerization process. As a matter of fact, if polymerization is stopped after 4 h for systems containing only MMA and nBA monomers, complete monomer conversion is observed with monomodal MMA/nBA particles of 91 nm (Figure 3A). On the other hand, when MMA, nBA, and FMA are utilized, after 4 h of polymerization, MMA/nBA particles are produced with residual FMA monomer. Thus, the reaction medium must be starved with respect to MMA and nBA, which allows for the diffusion of FMA facilitated by SDS/FSP during the next 5 h of the reaction. As a result, monomodal MMA/nBA/FMA colloidal particles are obtained through this two-stage reaction process, but their shape is nonspherical, as FMA is forced to locally polymerize on the surface of MMA/nBA. This is illustrated in Scheme 1, which pictorially depicts the rate of monomer conversion as a function of time. During the first stage, referred to as the saturation stage, the reaction vessel is saturated with all monomers and the reactivity ratios along with H_2O diffusivity are the determining factors of particle morphology. However, as the content of reactive monomers (MMA and nBA) is depleted, the system enters the starvation stage, where lesser reactive FMA monomer diffusion is facilitated by starving the system, increasing the time, and decreasing the surface tension of the aqueous phase. It should be noted that previous efforts in the preparation of F-containing colloidal dispersions oftentimes required pressurized reaction vessels, high agitation, cosolvents, or complex surfactant

Scheme 1. Schematic Illustration Depicting the Two-Stage Synthetic Process Producing MMA/nBA/FMA Colloidal Particles though Emulsion Polymerization

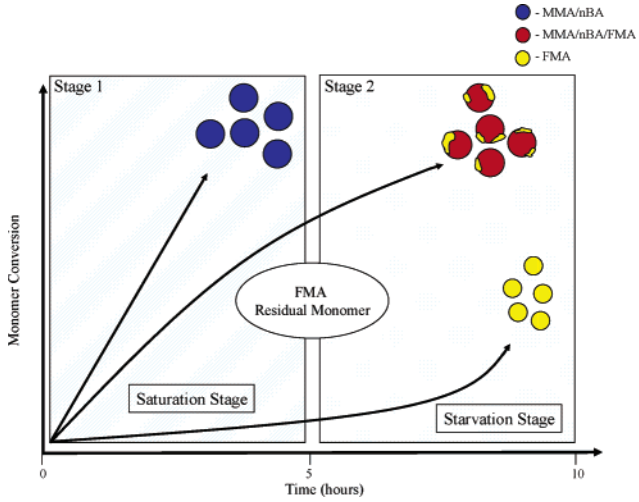

mixtures. In most cases, however, the resulting solids content was too low to form stable films. In the current study, the utilization of SDS/FSP surfactants provides suitable environments for diffusion and polymerization of FMA by the monomer-starved classical emulsion process by which the resulting solids content is sufficient for the production of stable colloidal dispersions and, equally important, uniform films offer particle coalescence.

With these data in mind, let us now focus on the role of particle morphologies and their low surface tension components in film formation. Similarly to the previous studies, we analyzed surface components using ATR-FTIR spectroscopy. Specifically, we are interested in mobility and stratification of individual components near the film−air (F−A) interface. Figures 4−7 show a series of polarized ATR-FTIR spectra recorded from 0.18 μm near the F−A interface of MMA/nBA films without FMA (Figure 4) and with 3.3% FMA (Figure 5), 5% FMA (Figure 6), and 8.5% FMA (Figure 7). Due to the fact that elevated temperatures have been shown to significantly impact the mobility of individual components,

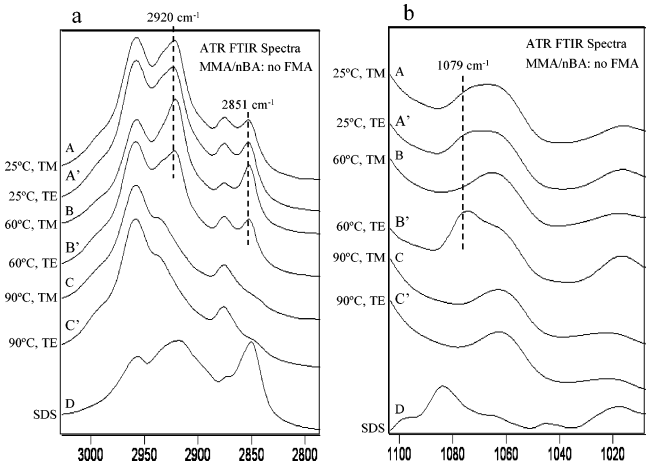

Figure 4. ATR-FTIR spectra recorded at 0.18 μm from the F−A interface in the spectral regions of 3000−2800 cm^{-1} (a) and 1100−1020 cm^{-1} (b) of MMA/nBA (A, and A′, TM and TE polarizations at 25 °C; B and B′, TM and TE polarizations at 60 °C; C and C′, TM and TE polarizations at 90 °C; D, SDS reference spectrum).

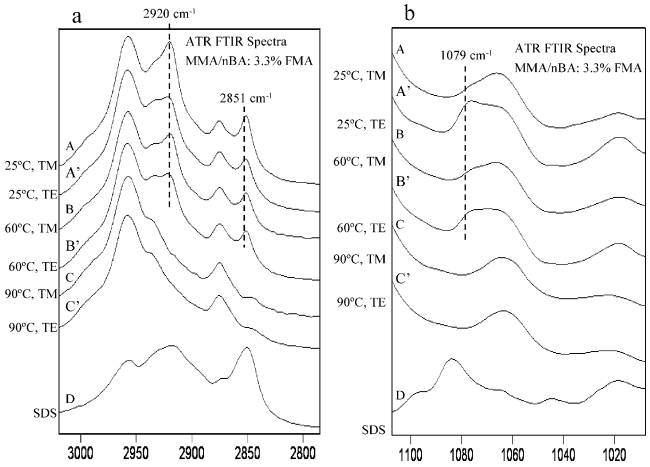

Figure 5. ATR-FTIR spectra recorded at 0.18 μm from the F−A interface in the spectral regions of 3000−2800 cm^{-1} (a) and 1100−1020 cm^{-1} (b) of MMA/nBA/FMA (3.3% w/w) (A and A′, TM and TE polarizations at 25 °C; B and B′, TM and TE polarizations at 60 °C; C and C′, TM and TE polarizations at 90 °C; D, SDS reference spectrum).

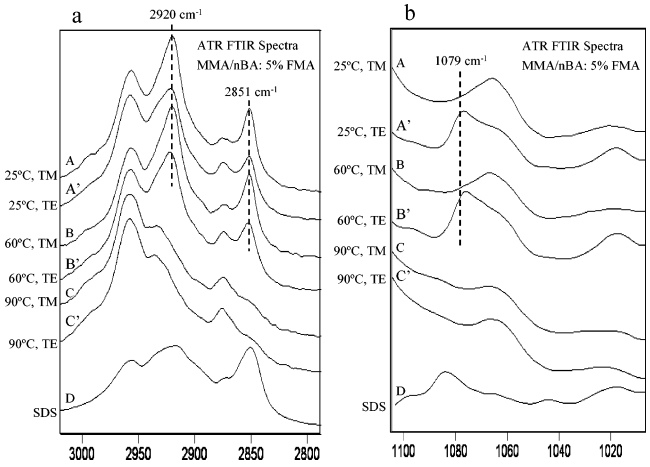

Figure 6. ATR-FTIR spectra recorded at 0.18 μm from the F−A interface in the spectral regions of 3000−2800 cm^{-1} (a) and 1100−1020 cm^{-1} (b) of MMA/nBA/FMA (5% w/w) (A and A′, TM and TE polarizations at 25 °C; B and B′, TM and TE polarizations at 60 °C; C and C′, TM and TE polarizations at 90 °C; D, SDS reference spectrum).

each film was annealed for 2 h at 25, 60, and 90 °C (traces A/A′, B/B′, and C/C′, respectively). For reference purposes, trace D in each figure represents the spectrum of SDS. Parts a and b of Figure 4 illustrate ATR-FTIR spectra in the C−H and S−O stretching regions of MMA/nBA, respectively. As shown in traces A/A′ of Figure 4a, SDS migrates to the F−A interface at 25 °C, as demonstrated by the presence of the 2920 and 2851 cm^{-1} C−H stretching bands of SDS. Since the spectra recorded using TE and TM polarizations exhibit the same intensities, hydrophobic tales of SDS display no preferential orientation near the F−A interface. However, annealing at 60 °C results in an increase of SDS concentration near the F−A interface, and furthermore, the increased intensity of the 2920 cm^{-1} IR band (Figure 4a, trace B) indicates that the hydrophobic tails are preferentially perpendicular. At the same time, the $-SO_3^-Na^+$ hydrophilic headgroups are parallel to the F−A interface (Figure 4b, trace B′). Further annealing at 90 °C (Figure 4, traces C and C′) results in no SDS at the F−A interface. It should be noted that previous

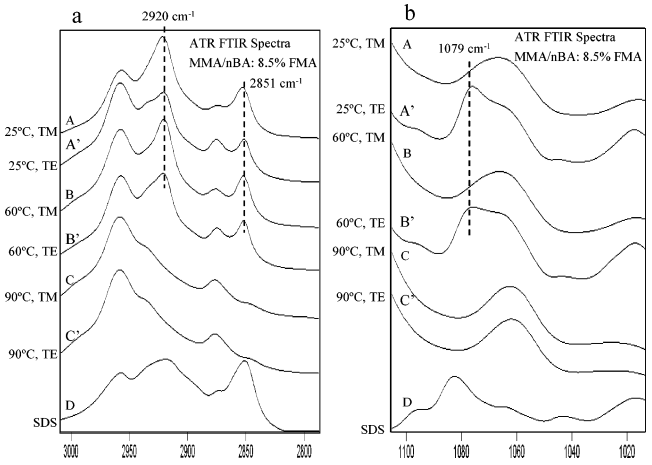

Figure 7. ATR-FTIR spectra recorded at 0.18 μm from the F−A interface in the spectral regions of 3000−2800 cm^{-1} (a) and 1100−1020 cm^{-1} (b) of MMA/nBA/FMA (8.5% w/w) (A and A′, TM and TE polarizations at 25 °C; B and B′, TM and TE polarizations at 60 °C; C and C′, TM and TE polarizations at 90 °C; D, SDS reference spectrum).

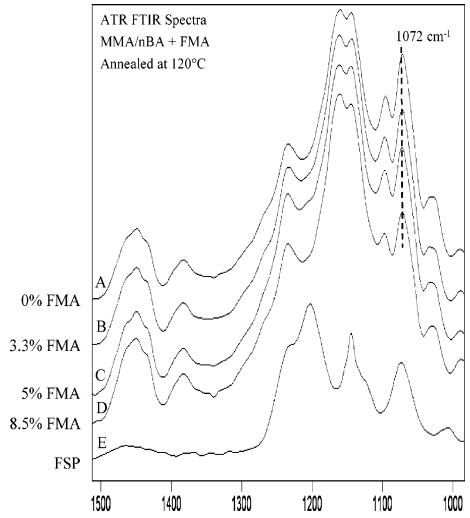

Figure 8. ATR-FTIR spectra recorded from 0.18 μm of copolymer films annealed at 120 °C: (A) MMA/nBA; (B) MMA/nBA/FMA (3.3% w/w FMA); (C) MMA/nBA/FMA (5% w/w FMA); (D) MMA/nBA/FMA (8.5% w/w FMA); (E) FSP reference spectrum.

studies on non-F-containing colloids showed that 120 °C was necessary for SDS to diffuse back into the film.[48]

Parts a and b of Figure 5 represent ATR-FTIR spectra recorded from the F−A interface of MMA/nBA/FMA copolymer films synthesized in the presence of SDS and FSP containing 3.3% (w/w) FMA. In contrast to MMA/nBA annealed at 25 °C, MMA/nBA/FMA (3.3%) films show a higher surface concentration of SDS at the F−A interface with its hydrophobic tails preferentially perpendicular to the F−A interface (Figure 5a, trace A), and the hydrophilic S−O headgroups parallel (Figure 5b, trace A′). Upon annealing at 60 °C (Figure 5, traces B and B′), SDS becomes randomly oriented and only minute traces are detected at the F−A interface. Annealing at 90 °C allows for SDS to migrate back into the bulk of the film, as demonstrated by the absence of the 2920 and 1079 cm^{-1} SDS bands in traces C and C′ of each figure. Parts a and b of Figures 6 and 7 illustrate ATR-FTIR spectra recorded from the F−A interface of MMA/nBA/FMA (5% w/w FMA) and MMA/nBA/FMA (8.5% w/w FMA), respectively. As shown, 25 °C is sufficient for SDS stratification near the F−A interface, 60 °C facilitates decreased SDS levels, and 90 °C produces surfaces with no SDS.

Comparison of spectroscopic data in Figures 4−7 indicates that higher pFMA content enhances concentration levels of SDS near the F−A interface at 25 °C, but 90 °C is sufficient for SDS to diffuse back to the bulk of the film. At this point, it should be noted that although one would anticipate that FSP should also diffuse to the F−A interface under these conditions, as it turns out, this is not the case. These observations indicate that MMA/nBA core components of nonspherical particles facilitate coalescence, whereas the block pFMA phase remains intact. When the same films are further annealed at 120 °C, ATR-FTIR analysis of spectra recorded from the F−A interface shows that an increasing copolymer content of FMA in MMA/nBA/FMA colloidal dispersions directly affects the migration of FSP. This is manifested in Figure 8, trace A, where in the environment of pMMA/nBA, the 1072 cm^{-1} P−O band due to FSP is enhanced, indicating that 120 °C facilitates migration of FSP to the F−A interface, where annealing temperatures of 25, 60, and 90 °C are not sufficient. The presence of FSP at the F−A interface results from its affinity to compensate for an excess in surface energy present in MMA/nBA colloidal particles.[49] On the other hand, for MMA/nBA/FMA (3.3% w/w), there is a decrease of surface energy due to the presence of the F-containing monomer which diminishes stratification of FSP, as demonstrated by a decrease of the 1072 cm^{-1} band in Figure 8, trace B. Upon further incorporation of FMA (5% and 8.5% w/w) into MMA/nBA (Figure 8, traces C and D), the FSP surface concentration further diminishes, which is attributed to the minimized overall surface energy of the polymeric films resulting in the presence of FMA. Thus, the driving force for FSP to migrate to the F−A interface becomes minimized.

In an effort to identify surface morphological features of films containing FMA, AFM experiments were conducted. Figure 9 shows a series of phase AFM images recorded from the F−A interface for MMA/nBA and MMA/nBA/FMA films containing 3.3%, 5%, and 8.5% FMA (w/w) which were coalesced at 25 °C. As seen, there are considerable differences. While image A due to MMA/nBA displays a continuous one-phase component attributed to pMMA/nBA at the F−A interface, image B (MMA/nBA/FMA, 3% w/w) displays the presence of high aspect ratio crystallites at the F−A interface, which increases for films containing 5% w/w FMA (Figure 9C). Although the crystallites retain a high aspect ratio morphology, they become even larger in size and more densely packed for MMA/nBA/FMA films containing 8.5% FMA (Figure 9D). As we recall Figure 8, FSP was detected at the F−A interface for MMA/nBA and MMA/nBA/FMA films only upon annealing at 120 °C. Furthermore, by increasing the FMA content, a decrease of the FSP surfactant was observed. In contrast, AFM data illustrate that an increase of surface concentration of the crystallites with an increase of FMA content is detected, which indicates enhanced mobility of FMA to the F−A interface at higher FMA concentration levels. Although one could argue that the presence of FSP and SDS may generate similar morphological features, previous studies[50] show that these species form mixed micelle−liquid crystalline domains, not rodlike crystallites shown in Figure 9. Considering these experimental observations and previous studies,[18,51] which

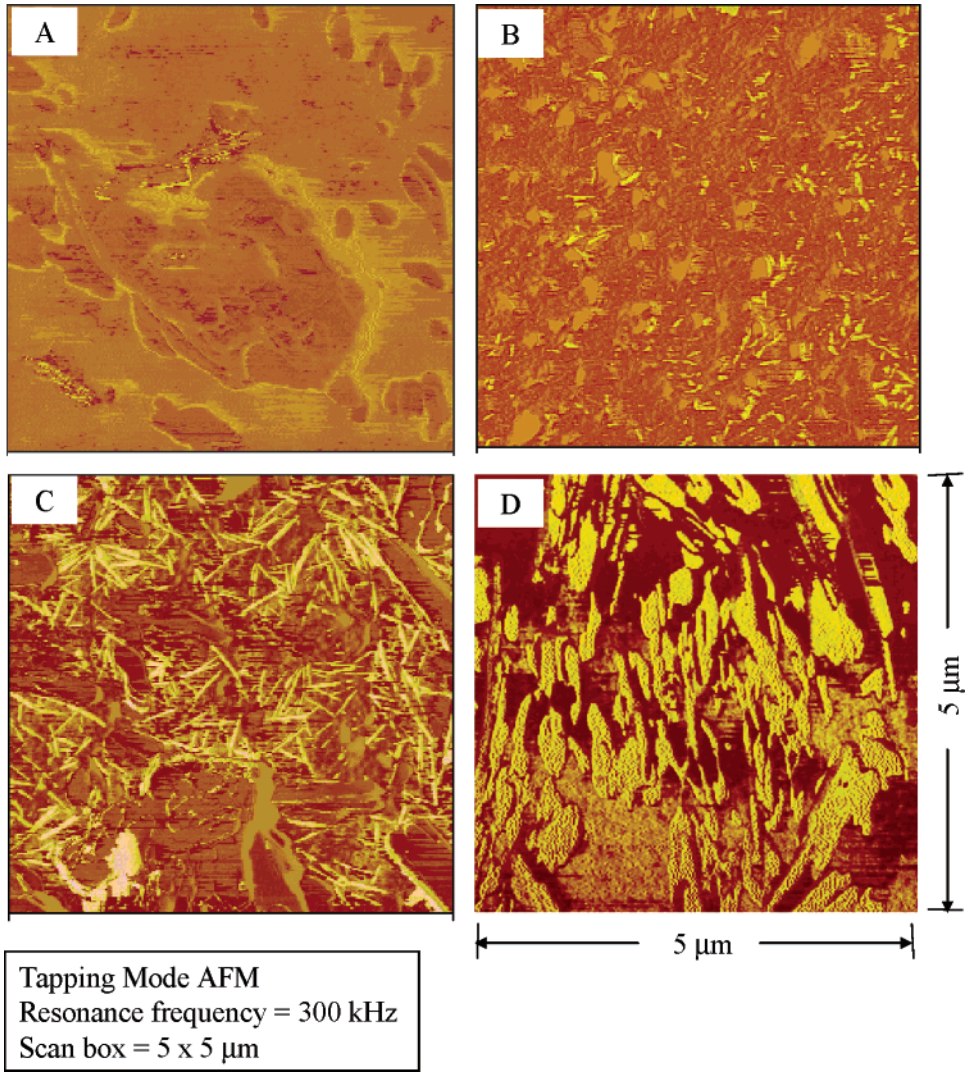

Figure 9. AFM phase images of copolymer films: (A) MMA/nBA; (B) MMA/nBA/FMA (3.3% w/w FMA); (C) MMA/nBA/FMA (5% w/w FMA); (D) MMA/nBA/FMA (8.5% w/w FMA). The scan box for each image is 5 μm × 5 μm.

have shown that C−F perfluoroalkyl side chains of sufficient length such as FMA are able to crystallize under ambient conditions, the formation of crystallites shown in Figure 9 is attributed to the stratification of FMA colloidal components of MMA/nBA/FMA particles during coalescence at 25 °C. Subsequently, the excess of pFMA near the F−A interface will lead to F-containing species obtained from colloidal particles.

Although these studies show that it is possible to control particle morphologies and stratification behaviors of individual components, it is also of interest to relate these findings to macroscopic properties. While the primary driving force for F-containing species to migrate to the F−A interface is their ability to compensate for the excess of the surface energy,[49] there are significant surface property changes. For example, we measured surface tension changes, solvent resistance, and changes of the kinetic coefficient of friction at the F−A interface, and the results are shown in Figure 10. As seen, the presence of pFMA at the F−A interface significantly alters the contact angle of a drop of water on the surface of each film. For MMA/nBA films, a contact angle of 69° was measured, whereas the addition of 3.3%, 5%, and 8.5% (w/w) FMA into the copolymer matrix increases the contact angles to 79°, 90°, and 100°, respectively. As anticipated, there is a decrease of the surface friction with an increase of FMA as well as an increase in solvent resiliency, and these data are also shown in Figure 10.

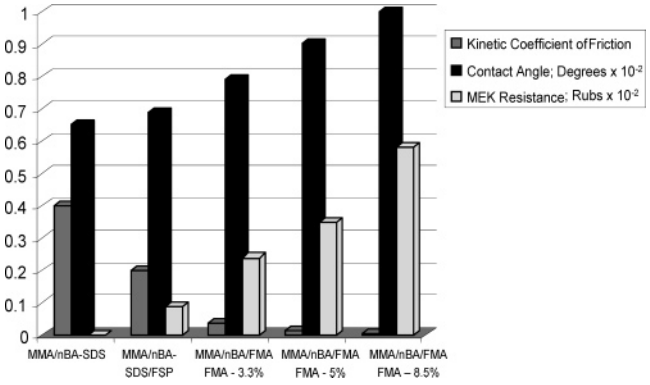

Figure 10. Kinetic coefficient of friction plotted as a function of colloidal composition. The same *y*-axis is used to plot contact angle measurements and MEK rub test results (values for both should be multiplied by 100).

Conclusions

The utilization of an SDS/FSP surfactant mixture allows for the synthesis of MMA/nBA/FMA colloidal dispersions under monomer-starved emulsion polymer-

ization conditions. The presence of FSP surfactant significantly decreases the surface tension of the aqueous phase, which facilitates F-containing monomer diffusion during polymerization. FMA diffuses at a slower rate than MMA and nBA, which gives rise to the synthesis of monomodal nonspherical colloidal particles possessing FMA blocks near the exterior of the MMA/nBA/FMA particles. The presence of FMA significantly decreases the surface concentration of FSP due to phase separation and subsequent reduction in the surface free energy at the F−A interface for the F-containing colloidal dispersions. The presence of crystallites at the F−A interface of MMA/nBA/FMA is attributed to stratification of the pFMA phase during coalescence, which offers significant enhancements in mechanical and chemical film stabilities.

Acknowledgment. We are thankful for support for these studies from the National Science Foundation Materials Research Science and Engineering Center (Grant No. DMR-0213883). The National Science Foundation Major Research Instrumentation program (Grant No. DMR-0315637) is also acknowledged. DuPont Co. is acknowledged for their generosity in supplying phosphoric acid bis(tridecafluorooctyl) ester ammonium salt (FSP) fluorosurfactant, and Dr. David Rice of Varian for his help in the NMR experiments.

References and Notes

(1) Chen, Y.; Ying, L.; Yu, j. W.; Kang, E.; Neoh, K. *Macromolecules* **2003**, *36*, 9451.
(2) Dargaville, T.; George, G.; Hill, D.; Whittacker, A. *Macromolecules* **2004**, *37*, 360.
(3) Deng, T.; Ha, Y.; Cheng, J.; Ross, C.; Thomas, E. *Langmuir* **2002**, *18*, 6719.
(4) Ding, L.; Olesik, S. *Macromolecules* **2003**, *36*, 4779.
(5) Fulton, J.; Deverman, G.; Yonker, C.; Grate, J.; De Yong, J.; McClain, J. *Polymer* **2004**, *44*, 3627.
(6) Gallyamoz, M.; Vinokur, R.; Nikitin, L.; Said-Galiyez, E.; Ernest, E.; Alexei, R.; Igor, V.; Schaumburg, K. *Langmuir* **2002**, *18*, 6928.
(7) Jin, J.; Smith, D.; Topping, C.; Suresh, S.; Chen, S.; Foulger, S.; Stephen, H.; Rice, N.; Nebo, J.; Mojazza, B. *Macromolecules* **2003**, *36*, 9000.
(8) Kang, S.; Luo, J.; Ma, H.; Barto, R.; Frank, C.; Dalton, L.; Jen, A. *Macromolecules* **2003**, *36*, 4355.
(9) Prabhakar, R.; Freeman, B.; Roman, I. *Macromolecules* **2004**, *37*, 7688.
(10) Sung, L.; Vicini, S.; Ho, D.; Hedhli, L.; Olmstead, C.; Kurt, W. *Polymer* **2004**, *45*, 6639.
(11) Borkar, S.; Siesler, H.; Hvilsted, S. *Macromolecules* **2004**, *37*, 788.
(12) Parker, H.; Lau, W.; Rosenlind, E. S. (Rohm and Haas Co.). U.S. Patent No. 6218464, 2001.
(13) Banks, R. E.; Smart, B. E.; Tatlow, J. C. *Organofluorine Chemistry Principles and Commercial Applications*; Plenum Press: New York, 1994.
(14) Hiyama, T. *Organofluorine Compounds*; Springer-Verlag: Berlin, 2000.
(15) Lovell, P. A.; El-Aasser, M. S. *Emulsion Polymerization and Emulsion Polymers*; John Wiley & Sons: New York, 1997.
(16) LoNostro, P.; Choi, S.; Ku, C.; Chen, S. *J. Phys. Chem. B* **1999**, *103*, 5347.
(17) Movchan, T.; Plotnikova, E.; Redina, L.; Gal'braikh, L.; Ys'yarov, O. *Colloid J.* **2003**, *65*, 47.
(18) Ha, J.; Park, I.; Lee, S.; Kim, D. *Macromolecules* **2002**, *35*, 6811.
(19) Cheng, S.; Chen, Y.; Chen, Z. *J. Appl. Polym. Sci.* **2002**, *85*, 1147.
(20) Barthelemy, P.; tomao, V.; Selb, J.; Chaudeir, Y.; Pucci, B. *Langmuir* **2002**, *18*, 2557.
(21) Kuwamura, S.; Hibi, T.; Agawa, T. *Waterborne & High-solids, and Powder Coatings Symopsium*, New Orleans, LA, The University of Southern Mississippi Press: Hattiesburg, MS, 1997; p 406.
(22) Kostov, G.; Ameduri, B.; Boutevin, B. *J. Fluorine Chem.* **2002**, *114*, 171.
(23) Huang, Z.; Shi, C.; Xu, J.; Kilic, S.; Enick, R.; Beckman, E. *Macromolecules* **2000**, *33*, 5437.
(24) Linemann, R. F.; Malner, T. E.; Brandsch, R.; Bar, G.; Ritter, W.; Mulhaupt, R. *Macromolecules* **1999**, *32*, 1715.
(25) Landfester, K.; Rothe, R.; Antonietti, M. *Macromolecules* **2002**, *35*, 1658.
(26) Fasick, R.; Raynolds, S. (E.I. DuPont de Nemours and Co.). U.S. Patent No. 3282905, 1966.
(27) Fasick, R.; Johnson, R. (E.I. DuPont de Nemors Co.). U.S. Patent No. 3378609, 1968.
(28) Raynolds, S.; Tandy, T. (E.I. DuPont de Nemours Co.). U.S. Patent No. 3462296, 1969.
(29) Kato, M.; Hiraharu, T.; Nishiwaki, K.; Tadenuma, H. (Japan Synthetic Rubber Co.). U.S. Patent No. 5349003, 1994.
(30) Kim, C. U.; Lee, J. M.; Ihm, S. K. *J. Appl. Polym. Sci.* **1999**, *73*, 777.
(31) Tsuda, N.; Iwakiri, Y.; Imoto, K.; Shimizu, Y.; Araki, T.; Kondo, M. (Daiken Industries, Ltd.). U.S. Patent No. 5804650, 1998.
(32) Yamana, M.; Uesugi, N.; Ogura, E. (Daikin Industries, Ltd.). U.S. Patent No. 6126846, 2000.
(33) Munekata, S. *Prog. Org. Coat.* **1988**, *16*, 113.
(34) Marion, P.; Beinert, G.; Juhue, D.; Lang, J. *J. Appl. Polym. Sci.* **1997**, *64*, 2409.
(35) Marion, P.; Beinert, G.; Juhue, D.; Lang, J. *Macromolecules* **1997**, *30*, 123.
(36) Thomas, R. R.; Lloyd, K. G.; Stika, L. M.; Stephans, L. E.; Magallanes, G. S.; Dimonie, V. L.; Sudol, E. D.; El-Aasser, M. S. *Macromolecules* **2000**, *33*, 8828.
(37) Adamson, A. W. *Physical Chemistry of Surfaces*, 2nd ed.; John Wiley & Sons: New York, 1967.
(38) Wu, S. *Polymer Interface and Adhesion*; Marcel Dekker: New York, 1982.
(39) Urban, M. W. *Attenuated Total Reflectance Spectroscopy of Polymers Theory and Practice*; American Chemical Society: Washington, DC, 1996.
(40) Urban, M. W. *Encylcopedia of Analytical Chemistry*; John Wiley & Sons: New York, 2000.
(41) Schaefer, J. S., E. O. Buchdahl, R. *Macromolecules* **1977**, *10*, 384−405.
(42) ASTM Standard Test D 1894-01.
(43) ASTM Standard Test D 5402-93.
(44) Liu, S. F.; Schmidt-Rohr, K. *Macromolecules* **2001**, *34*, 8416.
(45) Urban, M. W.; Provder, T. *Multidimensional Spectroscopy of Polymers*; American Chemical Society: Washington DC, 1995.
(46) Odian, G. *Principles of Polymerization*, 3rd ed.; John Wiley & Sons: New York, 1991.
(47) Brandrup, J.; Immergut, E. H. *Polymer Handbook*, 2nd ed.; John Wiley & Sons: New York, 1975.
(48) Dreher, W. R.; Zhang, P.; Urban, M. W.; Porzio, R. S.; Zhao, C. *Macromolecules* **2003**, *36*, 1228.
(49) Eastoe, J.; Rankin, A.; Wat, R.; Bain, C.; Styrkas, D.; Penfold, J. *Langmuir* **2003**, *19*, 7734.
(50) Dreher, W. R.; Urban, M. *Langmuir*, in press.
(51) Shafrin, E.; Zisman, W. *J. Phys. Chem.* **1962**, *66*, 740.

MA0479161